IEICE TRANS. FUNDAMENTALS, VOL.E96–A, NO.10 OCTOBER 2013

PAPER Special Section on Sparsity-aware Signal Processing

Image Restoration with Multiple DirLOTs

Natsuki AIZAWA[†a)], *Nonmember*, Shogo MURAMATSU[††], *Senior Member*, *and* Masahiro YUKAWA[†††], *Member*

SUMMARY A directional lapped orthogonal transform (DirLOT) is an orthonormal transform of which basis is allowed to be anisotropic with the symmetric, real-valued and compact-support property. Due to its directional property, DirLOT is superior to the existing separable transforms such as DCT and DWT in expressing diagonal edges and textures. The goal of this paper is to enhance the ability of DirLOT further. To achieve this goal, we propose a novel image restoration technique using multiple DirLOTs. This paper generalizes an image denoising technique in [1], and expands the application of multiple DirLOTs by introducing linear degradation operator P. The idea is to use multiple DirLOTs to construct a redundant dictionary. More precisely, the redundant dictionary is constructed as a union of symmetric orthonormal discrete wavelet transforms generated by DirLOTs. To select atoms fitting a target image from the dictionary, we formulate an image restoration problem as an ℓ_1-regularized least square problem, which can efficiently be solved by the iterative-shrinkage/thresholding algorithm (ISTA). The proposed technique is beneficial in expressing multiple directions of edges/textures. Simulation results show that the proposed technique significantly outperforms the non-subsampled Haar wavelet transform for deblurring, super-resolution, and inpainting.

key words: *DirLOT, deblurring, super-resolution, inpainting, iterative-shrinkage/thresholding algorithm (ISTA), multi-directional dictionary*

1. Introduction

High resolution displays are becoming in use in consumer appliances, e.g. 4K TV, and medical instruments. However, most of the present contents, such as digital terrestrial television broadcasting and a DVD image, are not fine enough to fill the resolution of such an advanced displays. Consider also a video surveillance system. A camera should take a photo or video which has enough resolution for detecting and analysing objects in frames, such as a person's face, even under inferior conditions. From these background, image restoration such as deblurring, super-resolution and inpainting are demanded in a lot of image and video processing applications. In order to solve these problems, we proposes to apply DirLOTs to image restoration. This paper is based on the article [2] and extended to include details of proposed dictionary and experimental results.

In this study, we deal with a common problem of image restoration, e.g. deblurring, super-resolution and inpainting [3]–[6]. Let $\mathbf{x} \in \mathbb{R}^J$ be an observed image which is represented by

$$\mathbf{x} = \mathbf{P}\mathbf{u}^* + \mathbf{w},$$

where $\mathbf{u}^* \in \mathbb{R}^I$ $(I \geq J)$ is an unknown original image, $\mathbf{P} \in \mathbb{R}^{J \times I}$ is a linear discrete operator which represents degradation and pixel loss through the measurement process, and $\mathbf{w} \in \mathbb{R}^J$ is a measurement noise modeled as a zero-mean additive white Gaussian noise (AWGN), respectively. Image restoration is a problem of finding a good candidate image $\hat{\mathbf{u}} \in \mathbb{R}^I$ of the unknown high-resolution clean image $\mathbf{u}^*$ only from the observed image $\mathbf{x}$. Since the operator $\mathbf{P}$ is in general not invertible, the problem is ill-posed. In this situation, sparsity works well for the solution. The framework of the problem setting is shown in Fig. 1. In the sparse representation approach, the candidate $\hat{\mathbf{u}}$ is expressed by a linear-combination of image prototypes (atoms) in a dictionary $\mathbf{D} \in \mathbb{R}^{I \times L}$, i.e. $\hat{\mathbf{u}} = \mathbf{D}\hat{\mathbf{y}}$, where $\hat{\mathbf{y}} \in \mathbb{R}^L$ is a candidate coefficient vector, and refers to the solution of an optimization problem.

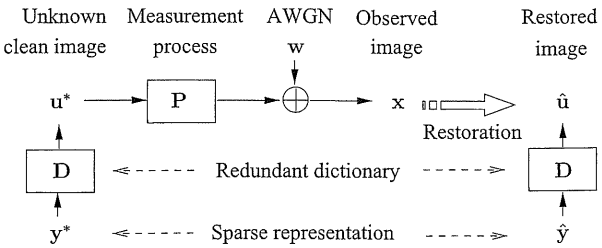

Fig. 1 Framework of image restoration problem setting.

The selection of dictionary $\mathbf{D}$, i.e. the modeling of the original signal $\mathbf{u}^*$, is a quite important task for solving the problem since it influences both of the restoration quality and the computational complexity. Recent development of image transforms involves non-separable ones for handling diagonal edges and textures since separable transforms are weak in representing such geometrical structures [5]. As a previous work, we have proposed 2-D non-separable DirLOTs [1]. The bases are allowed to be anisotropic with the fixed-critically-subsampling, overlapping, orthogonal, symmetric, real-valued and compact-support property. The hierarchical tree construction yields a two-dimensional directional symmetric orthonormal discrete wavelet transform (SOWT). In the articles [1], [7], [8], we adopted a union of the directional SOWTs (DirSOWTs) as a dictionary $\mathbf{D}$ so

Manuscript received January 21, 2013.
Manuscript revised May 2, 2013.

[†]The author is with the Graduate School of Science and Technology, Niigata University, Niigata-shi, 950-2181 Japan.
[††]The author is with the Dept. of Electrical and Electronic Engineering, Niigata University, Niigata-shi, 950-2181 Japan.
[†††]The author is with the Dept. of Electronics and Electrical Engineering, Keio University, Yokohama-shi, 223-8522 Japan.
a) E-mail: natsu@telecom0.eng.niigata-u.ac.jp

DOI: 10.1587/transfun.E96.A.1954

that we obtain an efficient image denoising technique.

In this paper, we propose a novel image restoration technique by using multiple DirLOTs and evaluate the performance of deblurring, super-resolution and inpainting. This paper is organized as follows: Section 2 reviews a union of directional SOWTs. Section 3 proposes an image restoration technique based on the dictionary, where we adopt ISTA as a solver [9]. Section 4 evaluates the performance of proposed method and verifies the significance. Finally, the conclusions follow in Sect. 5.

2. Union of Directional SOWTs

In this section, let us review DirLOTs, its hierarchical construction to obtain a DirSOWT and a union of DirSOWTs.

2.1 2-D Directional LOT (DirLOT)

DirLOTs are 2-D non-separable transforms and have a capability to be directional. A brief comparison of DirLOT with other transforms is shown in Table 1. Discrete cosine transform (DCT) [10] and discrete wavelet transform (DWT) [11] do not satisfy the overlapping, orthonormal and symmetric property simultaneously. On the other hand, DirLOTs have a special feature that the system simultaneously satisfies the fixed-critically-subsampled, overlapping, orthonormal, symmetric, real-valued and compact support property with a non-separable basis. As well, it can hold the trend vanishing moments (TVMs) for any direction and has an appropriate boundary operation [1], [12]. The directional property works well for diagonal textures and edges.

2.2 Lattice structure of 2-D DirLOT

Figure 2 shows the corresponding lattice structure of the analysis bank. Let $\mathbf{z} = (z_y, z_x)^T \in \mathbb{C}^2$ be a variable vector in the 2-D Z-transform domain. Then, the polyphase matrix of order $[N_y, N_x]^T$ is represented by the following product form [1]:

Table 1 Comparison among image transforms.

Property	GenLOT [10]	5/3,9/7 DWT [11]	Haar DWT [11]	DCT [10]	DirLOT [1]
Orthonormal	Yes	No	Yes	Yes	Yes
Symmetric	Yes	Yes	Yes	Yes	Yes
Overlapping	Yes	Yes	No	No	Yes
Directional	No	No	No	No	Yes

$$\mathbf{E}(\mathbf{z}) = \prod_{n_y=1}^{N_y} \left\{\mathbf{R}_{n_y}^{\{y\}}\mathbf{Q}(z_y)\right\} \cdot \prod_{n_x=1}^{N_x} \left\{\mathbf{R}_{n_x}^{\{x\}}\mathbf{Q}(z_x)\right\} \cdot \mathbf{R}_0\mathbf{E}_0, \quad (1)$$

where

$$\mathbf{Q}(z) = \frac{1}{2}\begin{pmatrix}\mathbf{I} & \mathbf{I}\\ \mathbf{I} & -\mathbf{I}\end{pmatrix}\begin{pmatrix}\mathbf{I} & \mathbf{O}\\ \mathbf{O} & z^{-1}\mathbf{I}\end{pmatrix}\begin{pmatrix}\mathbf{I} & \mathbf{I}\\ \mathbf{I} & -\mathbf{I}\end{pmatrix},$$

$$\mathbf{R}_0 = \begin{pmatrix}\mathbf{W}_0 & \mathbf{O}\\ \mathbf{O} & \mathbf{U}_0\end{pmatrix},$$

and

$$\mathbf{R}_n^{\{d\}} = \begin{pmatrix}\mathbf{I} & \mathbf{O}\\ \mathbf{O} & \mathbf{U}_n^{\{d\}}\end{pmatrix}.$$

In the above expression, the product of sequential matrices is defined by

$$\prod_{n=1}^{N} \mathbf{A}_n = \mathbf{A}_N\mathbf{A}_{N-1}\cdots\mathbf{A}_2\mathbf{A}_1.$$

$\mathbf{E}_0$ is an $M \times M$ symmetric orthonormal transform matrix given directly through the 2-D separable DCT, where M is the number of channels, i.e. $M = |\det(\mathbf{M})|$. Symbols $\mathbf{W}_0$, $\mathbf{U}_0$ and $\mathbf{U}_{n_d}^{\{d\}}$ denote orthonormal matrices of size $M/2 \times M/2$, which are freely controlled during the design process.

2.3 Design Examples

In the followings, the decimation matrix is set as $\mathbf{M} = \mathrm{diag}(M_y, M_x) = \mathrm{diag}(2, 2)$ in order to construct 2-D DWT trees, where $\mathrm{diag}(\cdot)$ denotes the diagonal matrix which has the argument vector as the diagonal elements. The support region of each analysis (or synthesis) filter results in $M_y(N_y + 1) \times M_x(N_x + 1)$. Figures 3 and 4 show design examples of DirLOTs of polyphase order $[N_y, N_x]^T = [4, 4]^T$. The design examples were obtained through the genetic algorithm function "ga" of MATLAB R2012a, where the following accumulated error energy was used as a cost function:

$$\sum_{m=0}^{3} \iint_{-\pi}^{\pi} \left\{\left|R_m\left(e^{j\omega_y}, e^{j\omega_x}\right)\right| - \left|H_m\left(e^{j\omega_y}, e^{j\omega_x}\right)\right|\right\}^2 d\omega_y d\omega_x,$$

where $R_m(e^{j\omega_y}, e^{j\omega_x})$ and $H_m(e^{j\omega_y}, e^{j\omega_x})$ are the frequency responses of the m-th reference and analysis filter, respectively. For a given TVM direction $\phi \in [-\frac{\pi}{4}, \frac{3\pi}{4})$, we define

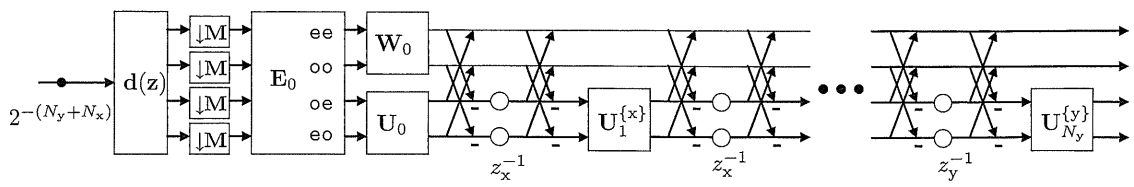

Fig. 2 Lattice structure of a four channel analysis bank of DirLOT, where $\mathbf{W}_0$, $\mathbf{U}_0$, $\mathbf{U}_n^{\{d\}}$ for $d \in \{x,y\}$ are parameter orthonormal matrices, $\mathbf{E}_0$ is an $M \times M$ matrix directly given by 2-D DCT, z_x^{-1} and z_y^{-1} are shifts of the coefficients in the horizontal and vertical direction, respectively.

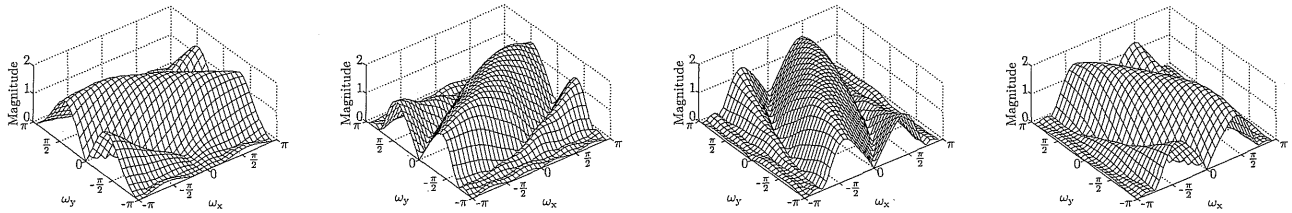

(a) $\phi = -\frac{\pi}{6}$[rad] (b) $\phi = \frac{\pi}{6}$[rad] (c) $\phi = \frac{2\pi}{6}$[rad] (d) $\phi = \frac{4\pi}{6}$[rad]

Fig. 3 Examples of amplitude responses $|H_0(e^{j\omega_y}, e^{j\omega_x})|$ of DirLOTs, where $[N_y, N_x]^T = [4, 4]^T$, i.e. the basis size is 10×10.

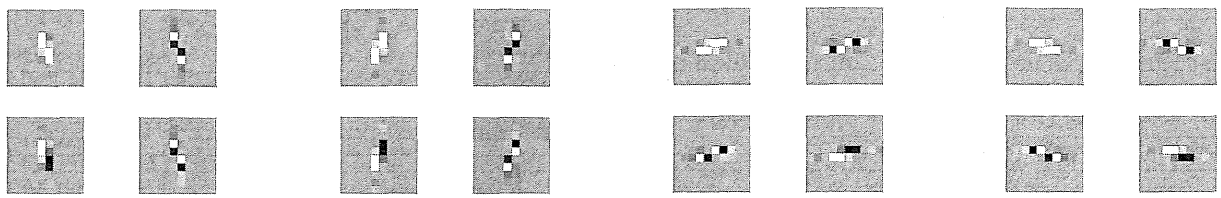

(a) $\phi = -\frac{\pi}{6}$[rad] (b) $\phi = \frac{\pi}{6}$[rad] (c) $\phi = \frac{2\pi}{6}$[rad] (d) $\phi = \frac{4\pi}{6}$[rad]

Fig. 4 Examples of bases of DirLOTs, where $[N_y, N_x]^T = [4, 4]^T$, i.e. the basis size is 10×10.

$R_0\left(e^{j\omega_y}, e^{j\omega_x}\right)$ by

$$R_0\left(e^{j\omega_y}, e^{j\omega_x}\right) = \begin{cases} B\left(e^{j\omega_y}, e^{j\omega_x}\right), & \phi \in \left\{0, \frac{\pi}{2}\right\}, \\ B\left(e^{j\omega_y}, e^{j(\omega_x - \omega_y \cot\phi)}\right), & \phi \in [-\frac{\pi}{4}, 0) \cup (0, \frac{\pi}{4}], \\ B\left(e^{j(\omega_y - \omega_x \tan\phi)}, e^{j\omega_x}\right), & \phi \in [\frac{\pi}{4}, \frac{\pi}{2}) \cup (\frac{\pi}{2}, \frac{3\pi}{4}], \end{cases}$$

where $B\left(e^{j\omega_y}, e^{j\omega_x}\right)$ is a 2-D maximally-flat frequency function $B\left(e^{j\omega_y}, e^{j\omega_x}\right) = 2A\left(e^{j\omega_y}\right)A\left(e^{j\omega_x}\right)$ defined through a 1-D maximally-flat frequency function

$$A\left(e^{j\omega}\right) = \left(\cos\frac{\omega}{2}\right)^{2P} \sum_{n=0}^{Q-1} d[n] \left(\sin\frac{\omega}{2}\right)^{2n},$$

where Q and P are the numbers of zeros at $\omega = 0$ and π, respectively, and the coefficients $d[n]$ are given by $d[n] = \frac{(P-1+n)!}{(P-1)!n!}$[13]. References $R_m\left(e^{j\omega_y}, e^{j\omega_x}\right)$ for $m = 1, 2, 3$ are specified by modulating $R_0\left(e^{j\omega_y}, e^{j\omega_x}\right)$ to $(\omega_y, \omega_x)^T = (\pi, \pi)^T$, $(0, \pi)^T$ and $(\pi, 0)^T$, respectively.

The design parameters for the examples shown in Figs. 3 and 4 are $P = Q = 3$ and $\phi \in \{-\pi/6, \pi/6, 2\pi/6, 4\pi/6\}$ [rad]. It is observed that the amplitude responses of $H_0(e^{j\omega_y}, e^{j\omega_x})$ are flat along the direction $\mathbf{u}_\phi^T = (\sin\phi, \cos\phi)$ at $\omega^T = (\omega_y, \omega_x) = (0, 0)$.

3. Proposed Image Restoration Technique Based on Multiple DirLOTs

We here propose to apply a union of multiple tree-structured DirLOTs, i.e. DirSOWTs, as $\mathbf{D}$ to image restoration problems shown in Fig. 1. Due to the measurement process $\mathbf{P}$, the matrix $\mathbf{A} = \mathbf{PD} \in \mathbb{R}^{J \times L} (J \leq L)$ which relates the observed image $\mathbf{x}$ to the coefficient vector $\mathbf{y}^*$ is no longer a tight frame, much less a union of unitary matrices, and the norms of the column vectors are not guaranteed to be unit. Among available methods to solve the problem, ISTA is a good candidate in the present case [9].

3.1 Problem Formulation

A single DirLOT is not suitable to represent multiple directional structures in images. In the followings, let us consider constructing a union of DirSOWTs (UDSW) as a dictionary $\mathbf{D}$ so that diagonal textures and edges are sparsely represented [1], [7], [8]. Our proposed dictionary $\mathbf{D}$ is represented by

$$\mathbf{D} = \left[\mathbf{\Phi}_{0\cup\frac{\pi}{2}}^T \quad \mathbf{\Phi}_{\phi_1}^T \quad \mathbf{\Phi}_{\phi_2}^T \quad \mathbf{\Phi}_{\phi_3}^T \quad \cdots \quad \mathbf{\Phi}_{\phi_{K-1}}^T\right], \tag{2}$$

where $\mathbf{\Phi}_{0\cup\frac{\pi}{2}}$ is a nondirectional symmetric orthonormal DWT with the classical two-order vanishing moments (VMs) as shown in Fig. 5 [14], [15], and $\mathbf{\Phi}_\phi$ is a DirSOWT constructed by a DirLOT with the two-order TVMs for the direction $\mathbf{u}_\phi$ [1]. K denotes the number of the DWTs, i.e. the redundancy of dictionary $\mathbf{D}$. Since $\mathbf{D}$ gives a tight frame with normalized atoms, $\mathbf{DD}^T = K\mathbf{I}$ holds [1], [16].

In the sparse representation approach, the candidate $\hat{\mathbf{u}}$ is expressed by a linear-combination of atoms in a dictionary $\mathbf{D} \in \mathbb{R}^{I \times L}$, i.e.

$$\hat{\mathbf{u}} = \mathbf{D}\hat{\mathbf{y}},$$

where $\hat{\mathbf{y}} \in \mathbb{R}^L$ is a candidate coefficient vector, and refers to the solution of the following form of optimization problem:

$$\hat{\mathbf{y}} = \arg\min_{\mathbf{y}} \|\mathbf{x} - \mathbf{PDy}\|_2^2 + \lambda\rho(\mathbf{y}), \tag{3}$$

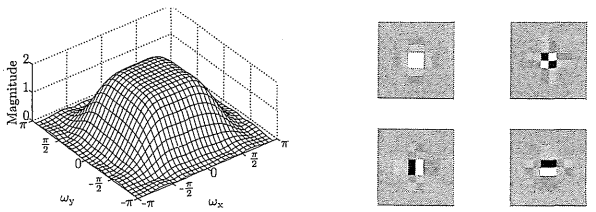

(a) $|H_0(e^{j\omega_y}, e^{j\omega_x})|$ (b) Basis

Fig. 5 A design example of nondirectional symmetric orthonormal DWT, where $[N_y, N_x]^T = [4, 4]^T$, i.e. the basis size is 10×10.

Data: Observed picture $\mathbf{x} \in \mathbb{R}^J$
Result: Restored picture $\hat{\mathbf{u}} \in \mathbb{R}^I$
Initialization;
$i \leftarrow 0$;
$\mathbf{y}^{(0)} \leftarrow \frac{1}{K}\mathbf{A}^T\mathbf{x}$;
Main iteration to find $\mathbf{y}$ that minimizes $f(\mathbf{y}) = \|\mathbf{x} - \mathbf{A}\mathbf{y}\|_2^2 + \lambda\|\mathbf{y}\|_1$;
repeat
  $i \leftarrow i + 1$;
  $\mathbf{y}^{(i)} \leftarrow \mathcal{T}_{\frac{\lambda}{\alpha}}\left(\mathbf{y}^{(i-1)} - \frac{2}{\alpha}\mathbf{A}^T(\mathbf{A}\mathbf{y}^{(i-1)} - \mathbf{x})\right)$;
until $\|\mathbf{y}^{(i)} - \mathbf{y}^{(i-1)}\|_2^2 / \|\mathbf{y}^{(i)}\|_2^2 < \epsilon$;
$\hat{\mathbf{u}} \leftarrow \mathbf{D}\mathbf{y}^{(i)}$;

Algorithm 1: ISTA, where $\mathbf{A} = \mathbf{P}\mathbf{D}$ and $\alpha = 2\lambda_{\max}(\mathbf{A}^T\mathbf{A}) = 2K\lambda_{\max}(\mathbf{P}^T\mathbf{P})$, i.e. the Lipschitz constant of the gradient of $\|\mathbf{x} - \mathbf{A}\mathbf{y}\|_2^2$ [9].

where $\|\cdot\|_2$ is the ℓ_2-norm of a vector, $\mathbf{y} \in \mathbb{R}^L$ is a coefficient vector, $\rho(\cdot)$ is a regularization term and $\lambda \geq 0$ is a scalar real parameter to control the trade-off between reconstruction fidelity and sparsity. The purpose of this formulation is to appropriately select atoms fitting a target image from the dictionary. When $\rho(\cdot)$ is a convex function, the proximal forward-backward algorithm can be used to solve Eq. (3) [9]. For $\rho(\mathbf{y}) = \|\mathbf{y}\|_1$, i.e. the ℓ_1-norm regularization, the solver reduces to the iterative shrinkage/thresholding algorithm (ISTA), which guarantees the convergence to an exact solution and applicable to large data such as images [9].

3.2 Numerical Algorithm

If we select the ℓ_1-norm as the sparsity measure $\rho(\cdot)$ in Eq. (3), we can use ISTA as the solver. ISTA with dictionary $\mathbf{D}$ is shown in Algorithm 1 [9], where $\mathcal{T}_\lambda(\cdot)$ is the vector function that performs the element-wise scalar soft-shrinkage operation

$$\mathcal{T}_\lambda(\mathbf{v}) = \mathrm{diag}(\mathrm{sign}(\mathbf{v})) \cdot (|\mathbf{v}| - \lambda\mathbf{1})_+,$$

where $\mathrm{sign}(\cdot)$ and $|\cdot|$ take the element-wise signs and absolute values, respectively, and $(\cdot)_+$ replaces negative elements to zeros and remains positive elements. The Lipschitz constant α is determined only by the degradation process since $\mathbf{D}$ constitutes a tight frame, $\mathbf{D}\mathbf{D}^T = K\mathbf{I}$ and then

$$\lambda_{\max}(\mathbf{A}^T\mathbf{A}) = \lambda_{\max}(\mathbf{A}\mathbf{A}^T) = K\lambda_{\max}(\mathbf{P}\mathbf{P}^T) = K\lambda_{\max}(\mathbf{P}^T\mathbf{P})$$

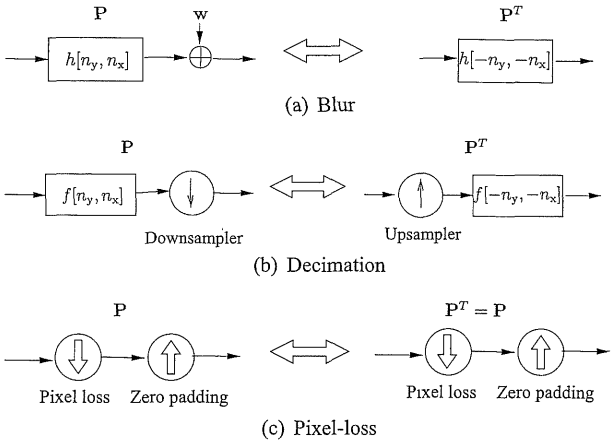

Fig. 6 Measurement processes with representative degradations and their adjoint operators.

holds, where $\lambda_{\max}(\cdot)$ denotes the maximum eigenvalue. Thus, the Lipschitz constant is given by

$$\alpha = 2K\lambda_{\max}(\mathbf{P}^T\mathbf{P}),$$

In Algorithm 1, we can use the fact that the dictionary $\mathbf{D}$ is decomposed into K orthonormal matrices and thus the parallel implementation is available.

3.3 Examples of Measurement Process

The linear operator $\mathbf{P}$ in Fig. 1 includes blur, decimation and/or pixel loss. Let us summarize the image restoration of these problems.

3.3.1 Deblurring

Deblurring is a problem to restore a clear picture from blurred one, where AWGN is often assumed. In the framework shown in Fig. 1, $\mathbf{P}$ is modeled as a convolution matrix which consists of the impulse response, i.e. point-spread-function (PSF), with spatial shifts. The adjoint operation with $\mathbf{P}^T$ required by ISTA is realized by the convolution with spatially reversal system, i.e. the 180-degree rotated version of PSF as shown in Fig. 6(a).

3.3.2 Super-Resolution

Super-resolution is a problem to restore a clear high-resolution picture from a decimated or low-resolution one. In Fig. 1, $\mathbf{P}$ is modeled as a convolution and downsampling matrix. The adjoint operation with $\mathbf{P}^T$ is composed of the upsampling and 180-degree-rotated convolution matrix. Figure 6(b) shows the pair of the operations.

3.3.3 Inpainting

Inpainting is a problem to restore missing pixels from the other observed remaining pixels. $\mathbf{P}$ is simply modeled as a diagonal matrix of which elements are either of 0 or 1, which

denote missing and remaining pixel position, respectively. Thus, the adjoint operation with $\mathbf{P}^T$ is exactly the same as $\mathbf{P}$ since $\mathbf{P}^T = \mathbf{P}$. Figure 6(c) shows the pair of the operations.

4. Simulation Results

This section shows some simulation results of deblurring, super-resolution and inpainting in order to verify the significance of our proposed dictionary UDSW. We perform simulation under the fixed iteration condition of 30 times. To assess the performance, the results of the ISTA-based image restoration is compared with those of the non-subsampled Haar wavelet transform (NSHT). The transforms adopted in this simulation are summarized in Table 2, where our proposed dictionary UDSW consists of a multiple DirSOWTs of $[N_y, N_x]^T = [4, 4]^T$. We select the following four angles for ϕ_k in Eq. (2) as

$$\phi_k \in \left\{-\frac{\pi}{6}, \frac{\pi}{6}, \frac{2\pi}{6}, \frac{4\pi}{6}\right\}.$$

Thus, the redundancy results in $K = 1 + 4 = 5$. The number of levels of each DWT is set to six. These parameters are experimentally selected. The basis termination method for the boundary operation is also applied [12]. On the other hand, the non-subsampled Haar wavelet transform adopted two-level construction, where the redundancy results in $K = 4 + 3 = 7$. In addition, we perform image restoration with some classical techniques as references.

Figure 7 shows original pictures used as unknown clean ones, $\mathbf{u}^*$. Tables 3 and 4 show the performance evaluations in terms of the peak-signal to noise ratio (PSNR) and structural similarity (SSIM) indeces. The SSIM index measures a similarity of two images, which approaches to one when the two images are perceptually close to each other [17]†.

Table 2 Adopted transforms and their features.

Abrv.	Features
NSHT	Two-level non-subsampled Haar DWT, separable, tight, nondirectional
UDSW	Union of six-level isotropic SOWT and DirSOWTs with two TVMs of $[N_y, N_x]^T = [4, 4]^T$, nonseparable, tight, multidirectional

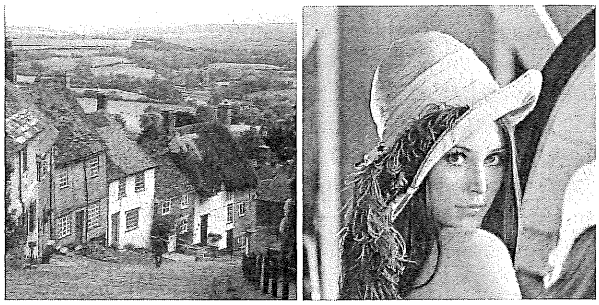

(a) *goldhill* (b) *lena*

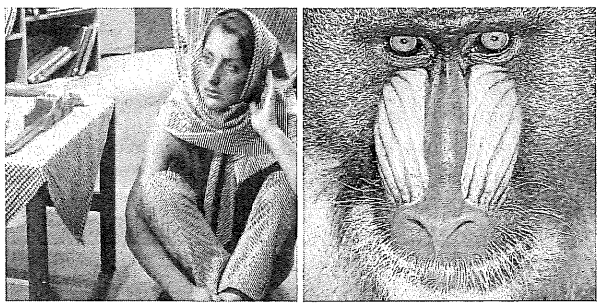

(c) *barbara* (d) *baboon*

Fig. 7 Original pictures $\mathbf{u}^*$ of size 512×512, 8-bit grayscale.

4.1 Deblurring

As the PSF $h[n_y, n_x]$, we used the 2-D Gaussian filter with standard deviation $\sigma_h = 2.0$. AWGN is also assumed with standard deviation $\sigma_n = 5$. Figs. 8, 9, 10 and 11 show observed pictures of "*goldhill*," "*lena*," "*barbara*" and "*baboon*" and three different restoration results of each picture. As a classical deblurring technique, we adopted the Wiener filter (MATLAB 'deconvwnr' function).

Table 3 Comparison of PSNRs among three methods for various pictures and measurement processes, where parameter λ, of which value is given in the parenthesis, is experimentally given. 'Classical' means Wiener, Bicubic and Median filter for deblurring, super-resolution and inpainting, respectively. The number of iterations is limited to 30.

Process	Picture	Classical	NSHT	UDSW
Deblurring	*goldhill*	24.41	28.45 (0.0011)	**28.47** (0.0028)
	lena	25.41	29.90 (0.0012)	**30.11** (0.0040)
	barbara	22.12	23.92 (0.0011)	**23.94** (0.0032)
	baboon	21.15	21.83 (0.0000)	21.83 (0.0001)
Super Resolution	*goldhill*	25.97	**29.11** (0.0003)	28.98 (0.0005)
	lena	26.98	**30.69** (0.0005)	30.60 (0.0010)
	barbara	22.91	**24.13** (0.0004)	24.10 (0.0004)
	baboon	20.84	**21.94** (0.0002)	21.93 (0.0003)
Inpainting	*goldhill*	23.64	16.18 (0.0447)	**29.66** (0.0940)
	lena	23.90	15.68 (0.0459)	**30.94** (0.1041)
	barbara	22.09	15.45 (0.0467)	**27.54** (0.1088)
	baboon	21.11	14.90 (0.0478)	**24.78** (0.1052)

Table 4 Comparison of SSIM indexes among three methods for various pictures and measurement processes, where parameter λ, of which value is given in the parenthesis, is experimentally given. 'Classical' means Wiener, Bicubic and Median filter for deblurring, super-resolution and inpainting, respectively. The number of iterations is limited to 30.

Process	Picture	Classical	NSHT	UDSW
Deblurring	*goldhill*	0.633	0.723 (0.0010)	**0.724** (0.0026)
	lena	0.666	0.796 (0.0012)	**0.821** (0.0059)
	barbara	0.543	0.657 (0.0010)	**0.668** (0.0044)
	baboon	0.517	0.528 (0.0002)	0.528 (0.0003)
Super Resolution	*goldhill*	0.682	**0.767** (0.0003)	0.759 (0.0004)
	lena	0.802	**0.859** (0.0003)	0.854 (0.0004)
	barbara	0.646	**0.700** (0.0003)	0.696 (0.0004)
	baboon	0.433	**0.547** (0.0002)	0.544 (0.0003)
Inpainting	*goldhill*	0.791	0.352 (0.0874)	**0.803** (0.0836)
	lena	0.808	0.289 (0.0948)	**0.856** (0.0873)
	barbara	0.791	0.379 (0.0722)	**0.845** (0.0896)
	baboon	0.758	0.397 (0.1032)	**0.769** (0.0824)

†MATLAB function ssim_index.m from http://www.cns.nyu.edu/~lcv/ssim/ was used.

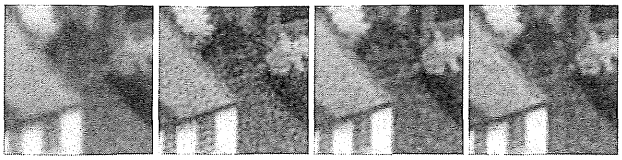

(a) Observed (b) Wiener (c) NSHT (d) UDSW

Fig. 8 Partial results of deblurring for "*goldhill.*"

(a) Observed (b) Wiener (c) NSHT (d) UDSW

Fig. 9 Partial results of deblurring for "*lena.*"

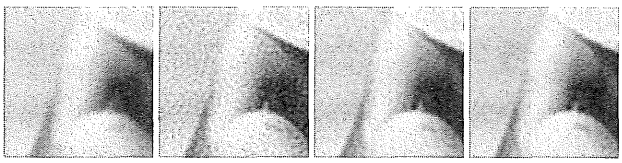

(a) Observed (b) Wiener (c) NSHT (d) UDSW

Fig. 10 Partial results of deblurring for "*barbara.*"

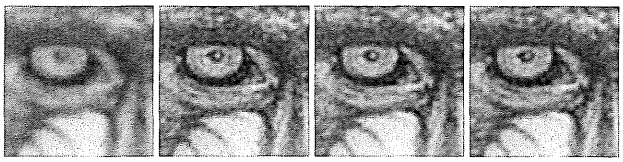

(a) Observed (b) Wiener (c) NSHT (d) UDSW

Fig. 11 Partial results of deblurring for "*baboon.*"

(a) Observed (b) Bicubic (c) NSHT (d) UDSW

Fig. 12 Partial results of super-resolution for "*goldhill.*"

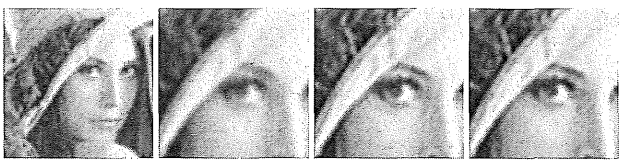

(a) Observed (b) Bicubic (c) NSHT (d) UDSW

Fig. 13 Partial results of super-resolution for "*lena.*"

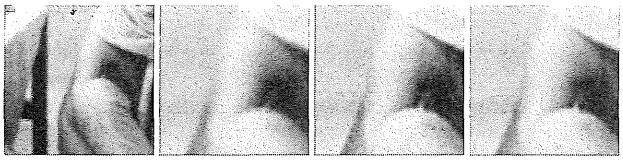

(a) Observed (b) Bicubic (c) NSHT (d) UDSW

Fig. 14 Partial results of super-resolution for "*barbara.*"

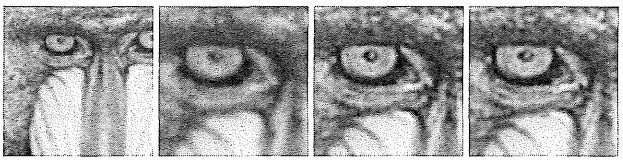

(a) Observed (b) Bicubic (c) NSHT (d) UDSW

Fig. 15 Partial results of super-resolution for "*baboon.*"

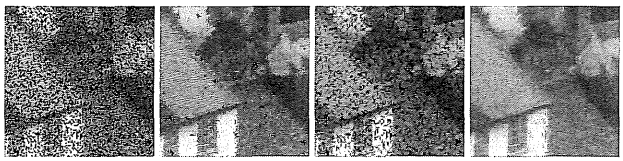

(a) Observed (b) Median (c) NSHT (d) UDSW

Fig. 16 Partial results of inpainting for "*goldhill.*"

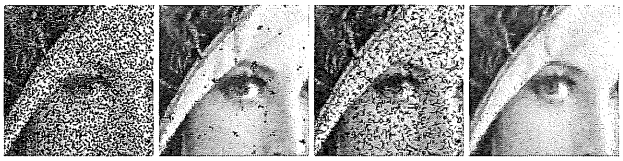

(a) Observed (b) Median (c) NSHT (d) UDSW

Fig. 17 Partial results of inpainting for "*lena.*"

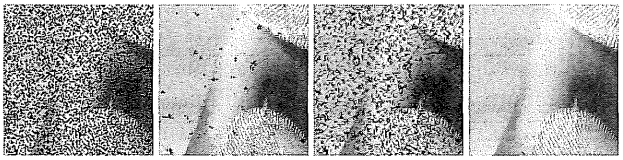

(a) Observed (b) Median (c) NSHT (d) UDSW

Fig. 18 Partial results of inpainting for "*barbara.*"

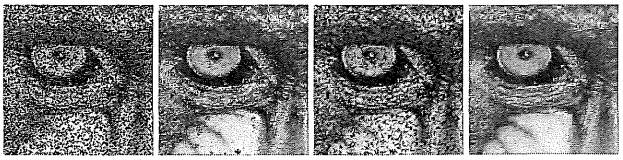

(a) Observed (b) Median (c) NSHT (d) UDSW

Fig. 19 Partial results of inpainting for "*baboon.*"

The results with UDSW have less degradation of texture than those with Wiener and NSHT. From Tables 3 and 4, it is observed that UDSW shows almost the best performance among three methods in terms of PSNR and SSIM index. From Figs. 20 and 21, it is observed that the performance of NSHT worsen as iteration increases, whereas the performance of UDSW is stable.

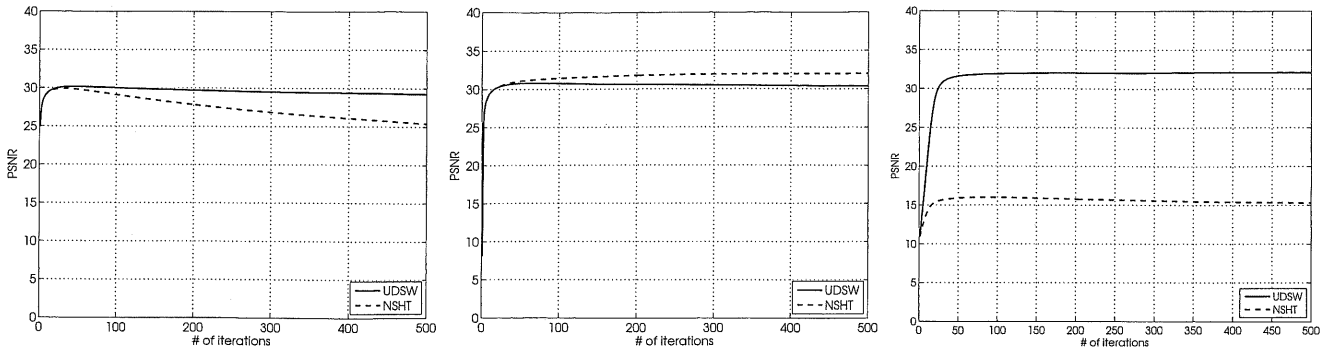

(a) Deblurring (b) Super-Resolution (c) Inpainting

Fig. 20 Comparison of convergence of UDSW and NSHT in PSNR. These simulation results are obtained for "*lena*."

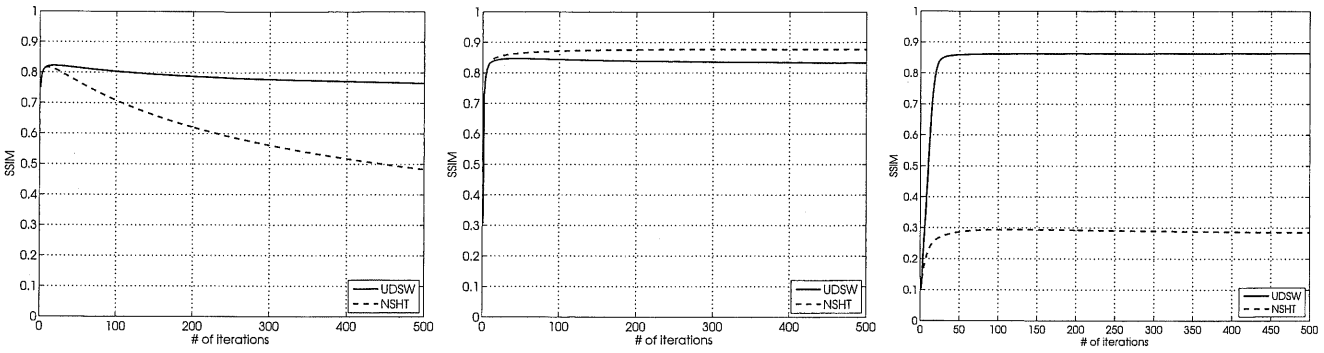

(a) Deblurring (b) Super-Resolution (c) Inpainting

Fig. 21 Comparison of convergence of UDSW and NSHT in SSIM. These simulation results are obtained for "*lena*."

4.2 Super Resolution

In this simulation, we assumed the 2-D Gaussian filter with standard deviation $\sigma_h = 2.0$ as a PSF $f[n_y, n_x]$ and the downsampling with factor two in every horizontal and vertical direction. Any noise is not explicitly added. In Figs. 12, 13, 14 and 15, the super-resolution performances are compared among three methods for "*goldhill*," "*lena*," "*barbara*" and "*baboon*." As a classical scaling-up technique, we used the bicubic interpolator (MATLAB '`imresize`' function).

From Tables 3 and 4, it is observed that the performances of NSHT and UDSW are comparable to each other and superior to the bicubic interpolation. The performance of NSHT is slightly superior to that of UDSW. Our conjecture is that the atoms of NSHT fit to the downsampling grid. Note that our proposed method archives these results with less redundancy.

4.3 Inpainting

Figures 16, 17, 18 and 19 compare the inpainting performances among three methods for "*goldhill*," "*lena*," "*barbara*," and "*baboon*." The observed picture in Figs. 16, 17, 18 and 19 lose 30% pixels randomly. As a classical approach to fill the lost pixels, we used the median filter (MATLAB '`medfilt2`' function) with the square window of size 5×5, while the other pixels are unchanged. The lost pixels are assumed to have zero values. Note that the ISTA-based restoration does not assume any value on the lost pixels. Any noise is not explicitly added. From Tables 3 and 4, UDSW shows significant performance improvement of inpainting. Our conjecture is that the atoms of NSHT have quite small region of support for inpainting.

From Figs. 20 and 21, the result with UDSW converges to a solution at about 100 iterations.

5. Conclusions

A novel image restoration technique was proposed by introducing a union of hierarchical DirLOTs. Through the application to deblurring, super-resolution and inpainting of images, it was shown that the proposed technique enjoys superior or comparable performance to the non-subsampled Haar wavelet transform with the ISTA-based approach. Last but not least, our proposed method achieves these results with less redundancy than that of the conventional dictionary.

Acknowledgment

This work was supported by JSPS KAKENHI (23560443). We would like to express our appreciation to Dr. Masao Yamagishi and Mr. Shunsuke Ono, Tokyo Institute of Technology, for their valuable comments.

References

[1] S. Muramatsu, D. Han, T. Kobayashi, and H. Kikuchi, "Directional lapped orthogonal transform: Theory and design," IEEE Trans. Image Process., vol.21, no.5, pp.2434–2448, May 2012.
[2] S. Muramatsu, N. Aizawa, and M. Yukawa, "Image restoration with union of directional orthonormal DWTs," Proc. of APSIPA, Dec. 2012.
[3] M. Elad, Sparse and Redundant Representations: From Theory to Applications in Signal and Image Processing, Springer, 2010.
[4] S. Mallat, A Wavelet Tour of Signal Processing, Third Edition: The Sparse Way, Academic Press, 2008.
[5] J.-L. Starck, F. Murtagh, and J.M. Fadili, Sparse Image and Signal Processing: Wavelets, Curvelets, Morphological Diversity, Cambridge University Press, 2010.
[6] B.K. Gunturk and X. Li, Image Restoration: Fundamentals and Advances, CRC Press, 2013.
[7] S. Muramatsu and D. Han, "Image denoising with union of directional orthonormal DWTs," Proc. IEEE ICASSP, pp.1089–1092, March 2012.
[8] S. Muramatsu, "SURE-LET image denoising with multiple directional LOTs," IEEE Proc. PCS, May 2012.
[9] D.P. Palomar and Y.C. Eldar, Eds., Convex Optimization in Signal Processing and Communications, Cambridge University Press, 2010.
[10] K.R. Rao and P.C.L. Yip, The Transform and Data Compression Handbook, Crc Pr I Llc, 2000.
[11] D.S. Taubman and M.W. Marcellin, JPEG2000, Image Compression Fundamentals, Standards and Practice, Kluwer Academic Publishers, 2002.
[12] S. Muramatsu, T. Kobayashi, M. Hiki, and H. Kikuchi, "Boundary operation of 2-D non-separable linear-phase paraunitary filter banks," IEEE Trans. Image Process., vol.21, no.4, pp.2314–2318, April 2012.
[13] P.P. Vaidyanathan, "On maximally-flat linear-phase FIR filters," IEEE Trans. Circuits Syst., vol.31, no.9, pp.830–832, Sept. 1984.
[14] A. Adachi, S. Muramatsu, and H. Kikuchi, "Constraints of second-order vanishing moments on lattice structures for non-separable orthogonal symmetric wavelets," IEICE Trans. Fundamentals, vol.E92-A, no.3, pp.788–797, March 2009.
[15] T. Kobayashi, S. Muramatsu, and H. Kikuchi, "Two-degree vanishing moments on 2-D non-separable GenLOT," IEEE Proc. ISPACS, pp.248–251, Dec. 2009.
[16] M. Elad, "Why simple shrinkage is still relevant for redundant representations?," IEEE Trans. Inf. Theory, vol.52, no.12, pp.5559–5569, Dec. 2006.
[17] Z. Wang, A.C. Bovik, H.R. Sheikh, and E.P. Simoncelli, "Image quality assessment: From error visibility to structural similarity," IEEE Trans. Image Process., vol.13, no.4, pp.600–612, April 2004.

Natsuki Aizawa received B.E. degree in electrical and electronic engineering from Niigata University in 2012. She is currently registered at graduate school of Niigata University. Her research interests are in image processing. She received the Incentive Award from the 25th Workshop on Circuits and Systems in 2012.

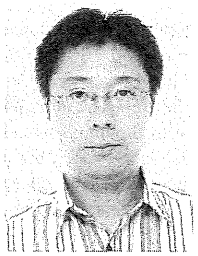

Shogo Muramatsu received the B.E, M.E. and Ph.D. degrees from Tokyo Metropolitan University in 1993, 1995 and 1998, respectively. From 1997 to 1999, he worked at Tokyo Metropolitan University. In 1999, he joined Niigata University, where he is currently an associate professor in Department of Electrical and Electronics Engineering, Faculty of Engineering. During year from 2003 to 2004, he was a visiting researcher at University of Florence, Italy. He is an Associate Editor for IEICE Transactions on Fundamentals of Electronics, Communications and Computer Sciences. His research interests are in multidimensional signal processing, multirate systems, image processing, video analysis and embedded vision systems. He is an Associate Editor for IEICE Transactions on Fundamentals of Electronics, Communications and Computer Science. Dr. Muramatsu is a member of IEEE(Institute of Electrical and Electronics Engineers, Inc.) and ITE(Institute of Image Information and Television Engineers of Japan).

Masahiro Yukawa received the B.E., M.E., and Ph.D. degrees from Tokyo Institute of Technology in 2002, 2004, and 2006, respectively. After studying as a Visiting Researcher at the University of York, U.K., from October 2006 to March 2007, he worked as a Special Postdoctoral Researcher for the Next Generation Mobile Communications Laboratory at RIKEN, Saitama, Japan, from April 2007 to March 2008, and for the Brain Science Institute at RIKEN from April 2008 to March 2010. From August to November 2008, he was a Guest Researcher at the Associate Institute for Signal Processing, the Technical University of Munich, Germany. He was an Associate Professor at the Department of Electrical and Electronic Engineering, Niigata University, Japan, from April 2010 to March 2013. He is currently an Assistant Professor at the Department of Electronics and Electrical Engineering, Keio University, Japan. His current research interests are in mathematical signal processing, nonlinear adaptive filtering, and sparse signal processing. He serves as an Associate Editor for IEICE Transactions on Fundamentals of Electronics, Communications and Computer Sciences, and the Journal of Multidimensional Systems and Signal Processing, Springer. From April 2005 to March 2007, he was a recipient of the Research Fellowship of the Japan Society for the Promotion of Science (JSPS). He received the Excellent Paper Award and the Young Researcher Award from the IEICE in 2006 and in 2010, respectively, the Yasujiro Niwa Outstanding Paper Award from Tokyo Denki University in 2007, and the Ericsson Young Scientist Award from Nippon Ericsson in 2009. He is a member of the Institute of Electrical and Electronics Engineers (IEEE).